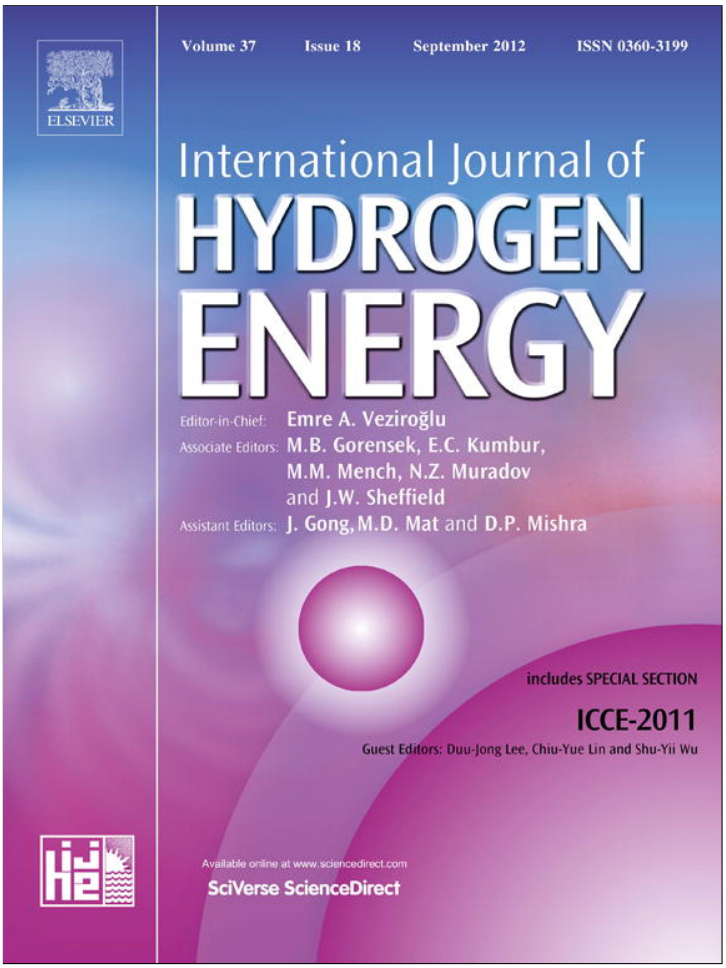

INTERNATIONAL JOURNAL OF HYDROGEN ENERGY 37 (2012) 13522–13528

Available online at www.sciencedirect.com

SciVerse ScienceDirect

journal homepage: www.elsevier.com/locate/he

Synthesis and evaluation of ATO as a support for Pt–IrO_2 in a unitized regenerative fuel cell

J.C. Cruz [a], S. Rivas [b], D. Beltran [a], Y. Meas [a], R. Ornelas [c], G. Osorio-Monreal [a], L. Ortiz-Frade [a], J. Ledesma-García [d], L.G. Arriaga [a,*]

[a] Centro de Investigación y Desarrollo Tecnológico en Electroquímica S.C., Parque Tecnológico Querétaro, Sanfandila, 76703 Pedro Escobedo, Querétaro, Mexico

[b] Centro de Investigación en Energía, Privada Xochicalco s/n, 62580 Temixco, Morelos, Mexico

[c] Tozzi Renewable Energy SpA, Via Zuccherificio, 10-48010 Mezzano (RA), Italy

[d] Universidad Autónoma de Querétaro, División de Investigación y Posgrado, Facultad de Ingeniería, 76010 Querétaro, Mexico

ARTICLE INFO

Article history:
Received 27 April 2012
Received in revised form
8 June 2012
Accepted 26 June 2012
Available online 17 July 2012

Keywords:
Water electrolysis
ATO support
Unitized regenerative fuel cell
Oxygen evolution
Oxygen reduction

ABSTRACT

An IrO_2 catalyst was prepared using a colloidal method followed by a thermal treatment. The catalyst was later mixed with Pt-Black and supported on the Sb-doped SnO_2 (ATO), synthesized through the same colloidal method. ATO was investigated as a possible catalyst support in an electrode of a regenerative fuel cell (URFC), where Pt–IrO_2 was used as the catalyst for the oxygen evolution and reduction reactions. The morphology and composition of the ATO support was investigated through transmission electron microscopy, X-ray diffraction (including Rietveld Refinement), BET analysis, and X-ray fluorescence. An ATO support was obtained with a highly homogeneous distribution and crystal sizes, measuring approximately 4–6 nm.

The Pt–IrO_2/ATO material was deposited on a Nafion 115 membrane with 0.5 mg cm^{-2} of catalyst loading. Pt/Vulcan XC-72 (30 wt. %, E-TEK) was used as the catalyst in the H_2 compartment with a Pt loading of 0.4 mg cm^{-2}. The electrochemical activity of the Pt–IrO_2/ATO for oxygen evolution/reduction in the URFC system was investigated by AC-impedance spectroscopy, linear voltammetry, and chronoamperometry techniques. The maximum mass current activity was 1118 A g^{-1} at 1.8 V in proton-exchange membrane water electrolyser mode (PEMWE) and 565 A g^{-1} at 0.3 V in proton-exchange membrane fuel cell mode (PEMFC), both at 80 °C. The value of the round-trip energy efficiency was approximately 48% at 50 A g^{-1}.

1. Introduction

Electrolysers and fuel cells are the most promising technologies for production and utilization of hydrogen as an energy storage medium [1–9]. Both systems may alternatively operate in the same device based on a proton-exchange membrane (PEM). The combination of both processes in the same system is known as unitized regenerative fuel cell (PEM-URFC). URFC devices are characterized by a fast startup, efficient operation at low temperature without significant power

* Corresponding author. Tel.: +52 4422116069; fax: +52 4422116008.
E-mail address: larriaga@cideteq.mx (L.G. Arriaga).

0360-3199/$ – see front matter
http://dx.doi.org/10.1016/j.ijhydene.2012.06.095

consumption and stable operation, even after a large number of startup/shutdown cycles.

During hydrogen production by water electrolysis in PEM system (PEMWE), most of the overpotential responsible for losses is related to the electrochemical processes at the anode, where the O_2 evolution reaction takes place [10]. RuO_2 is considered the most efficient catalyst for the oxygen evolution reaction (OER) in the alkaline electrolyte [11–13]; however, in acidic media, RuO_2 undergoes strong degradation during O_2 evolution with a consequent loss of its chemical reactivity. RuO_2 can form different sub-oxides that affect its stability and the registered overpotentials [14]. Certain materials, such as IrO_2, are used as catalysts due to their similar properties to those of RuO_2. It is even possible to use chemical mixtures of both oxides at different ratios [2,15,16].

In fuel cell mode (PEMFC), the limiting process occurs at the cathode, where the oxygen reduction reaction (ORR) takes place on metal electrodes, such as Pt, Pd, Ru, Ir, Rh, Au, and alloys [17,18] in acidic environments.

One of the challenges for the PEM-URFC is the development of new catalyst supports that can reduce the catalytic loading of the materials and increase their stability in PEMWE systems, where carbon-based materials are subjected to high potentials, humidity and temperatures that will accelerate the corrosion process. Such characteristics as high surface area, good electrical conductivity, and high resistance to corrosion at a range of potentials between 0 and 2 V are required for a catalyst support with this potential application.

A number of materials with attractive features as catalyst support have already been used, such as M–TiO_2, WO_3, S–ZrO_2, Sn–In_2O_3, WC, and Ti_nO_{2n-1} [19–30]. The most common for OER is the Ebonex® (Atraverda Ltd., UK), which consists of an electrically conductive ceramic material based on titanium sub-oxides, mainly Ti_4O_7 and Ti_5O_9. These sub-oxides are the main conductive compounds in a homologous series of crystallographic shear structures with the general formula Ti_nO_{2n-1} ($4 \leq n \leq 10$), known as the Magneli phase [30]. Recent studies have shown the potential use of this material as a catalyst support for the OER and the ORR [31–33]; however, this material has low surface area (1.7 $m^2\ g^{-1}$) compared with Vulcan XC-72 (205 $m^2\ g^{-1}$) [32,34].

Another material that has shown potential as a catalyst support is Sb-doped SnO_2 (ATO), due to its low electrical resistance (10^{-2}–10^{-3} Ω cm) compared with Ebonex® (10^{-3} Ω cm) [35] and its enhanced surface area. Another unique feature is its stability in acidic media [36]. Recent studies have reported the use of commercial ATO (Sigma–Aldrich) with a surface area of 47 $m^2\ g^{-1}$ and average particle size of 30–40 nm, which resulted in a high distribution of catalytic material available for the OER in PEMWE mode [37,38]. This paper presents the synthesis and evaluation of ATO with a surface area value superior to commercial ATO, and compares its performance as a catalyst support for dual-functions mixed with Pt–IrO_2 as a catalyst in a PEM-URFC. ATO was synthesized and characterized by physicochemical and electrochemical techniques as a dual-function catalyst support for PEMFC and PEMWE modes. Conversion efficiencies and performance in the PEM-URFC cell were determined and compared with previously reported results obtained with Ebonex® as the catalyst support.

2. Experimental

2.1. Synthesis of the ATO support

The ATO material was synthesized by dissolving 2.65 g of $SnCl_4.5H_2O$ (Strem chemical) in 20 mL of HCl, then heating (60 °C) and stirring during 30 min. At the same time 0.187 g of $SbCl_3$ (Strem) was dissolved in 2 mL of HCl. Both solutions were mixed during 20 min and subsequently combined with a 1:1 ethanol:isopropanol mixture, under air atmosphere and magnetically stirred for 4 h. The sample was heated (≤75 °C) to obtain a precipitate and then calcined at 500 °C for 12 h.

2.2. Preparation of Pt–IrO_2/ATO

Synthesis procedure of IrO_2 has previously been reported [15]. A sample of IrO_2 was mixed mechanically with Pt-black (E-TEK) 50:50 wt.%. Afterwards, the catalysts were supported (in a 30% wt. ratio) on Sb-doped SnO_2 (ATO) by sonication, in an ultrasonic bath of isopropanol at 80 °C, until a dry powder was obtained. This powder was subsequently crushed and mixed with a 33% Nafion® solution (Electrochem, 5% in isopropanol) for later deposition on a Nafion 115 membrane.

2.3. Physicochemical characterization of ATO

X-ray diffraction (XRD) was performed in a Rigaku DMAX-2200 diffractometer, using CuKα radiation at 40 kV and 40 mA. The diffractometer was operated at 0.08° min^{-1}. The collected data were refined by the Rietveld method using FULLPROF SUITE software [39,40]. The Thompson-Cox-Hastings pseudo-Voight function was used to model peak shapes and preferred orientation. The background was modeled as a polynomial with 6 refined coefficients. The diffraction patterns were fitted to the JCPDS (Joint Committee on Powder Diffraction Standards) database. The surface area of the ATO was estimated according to the Barrett–Joiner–Halenda (BJH) method, which was then used for the determination of the cumulative area and the pore sizes measured in an Autosorb® IQ Gas Sorption Analyzer (Quantachrome).

X-ray fluorescence analysis (XRF) of the catalysts was carried out in a Bruker AXS S4 Explorer spectrometer, operating at a power of 1 kW and equipped with a Rh X-ray source, a LiF220 crystal analyzer, and a 0.12° divergence collimator. The morphology of the ATO support was investigated with a Phillips TEM microscope Model CM200 operated at 200 kV. The TEM samples were prepared by dispersing the ATO in isopropyl alcohol by ultrasonic treatment dropping the suspension onto carbon-coated grids.

2.4. Preparation of membrane-electrode assembly (MEA)

A Nafion 115 (Ion Power) membrane was used as solid polymer electrolyte. The oxygen reduction/evolution catalyst supported in ATO was directly deposited onto one side of the membrane using a hot-spray technique. Inks were composed of aqueous dispersions of the catalyst, catalyst support, deionised water, Nafion® solution (5% Aldrich), and anhydrous Ethanol (J.T. Baker); Pt–IrO_2 (50:50 wt.%) catalyst loading

was 0.5 mg cm^{-2}. A commercial 30% Pt/Vulcan XC-72 (E-TEK, PEMEAS, Boston, USA) was used as the catalyst for the dual-functional hydrogen electrode. The hydrogen electrode catalyst ink was prepared by mixing a suspension of Nafion ionomer in water with the Pt/C catalyst powder [41,42] in an ultrasonic bath. The obtained ink was spread on carbon cloth backings (GDL ELAT from E-TEK) with a Pt loading of 0.4 mg cm^{-2}. The ionomer content in both electrodes was 33 wt.% in the catalytic layer after drying. The geometrical area of the electrode was 5 cm^2. The MEA was directly installed in the cell housing and compressed by tightening to 9 N m using a dynamometric wrench.

2.5. *Electrochemical characterization of MEA*

URFC electrochemical behavior was evaluated by linear voltammetry, chronoamperometry and electrochemical impedance spectroscopy (EIS) in a frequency range of 10 kHz to 1 Hz. The electrochemical characterization was performed with a PGSTAT Autolab 302 Potentiostat/Galvanostat equipped with a booster of 20 A (Metrohm®) and a Frequency Response Analyser (FRA). The fuel cell test station, which operated on liquid fuel (ElectroChem Inc. with a direct methanol unit couple), was used to control operating parameters, such as cell temperature, inlet temperature of gases and liquids, gas humidity, pressure, and flow rate.

The electrolyser performance was evaluated at 80 °C. Deionised water was circulated at 2 mL min^{-1} in the oxygen electrode compartment. Linear voltammetry profiles in PEMWE mode were performed for a range of potentials from 1 to 1.8 V at a 50 mV s^{-1} scan rate. The fuel cell performance test was carried out under atmospheric pressure at 80 °C by feeding dry H_2 and air, at 50 and 100 scc of flow, respectively. The linear voltammetry curves in PEMFC mode were performed from open circuit voltage (OCV) to 0.3 V with a 50 mV s^{-1} scan rate.

3. Results and discussion

Fig. 1 shows the obtained diffraction pattern of the ATO support with its corresponding Rietveld refinement. From this analysis, it was possible to identify $Sn_{0.90}Sb_{0.1}O_2$ in the rutile phase (JCPDS 88–2348). Presented in this figure are the observed pattern (Yobs), the calculated pattern (Ycalc), the difference between them (Yobs-Ycalc), and their corresponding Bragg positions. Good coherence between the experimental and calculated diffraction pattern were observed.

The mean crystallite size was estimated from the broadening of the main peaks using the Debye–Scherrer equation. Particle dimensions of 4–6 nm were obtained for the ATO support. These sizes are smaller than those reported for commercial ATO supports [37]. To verify the presence of Sb in the support, an XRF study was conducted which yielded the results listed in Table 1. The ratio between Sn and Sb is approximately 10:1. During the XRF testing, chloride ions were also detected, at levels below 1%, these ions can appear as contaminants during the reactions of interest. Even though the synthesized ATO was washed several times, it is not possible to eliminate this contaminant completely.

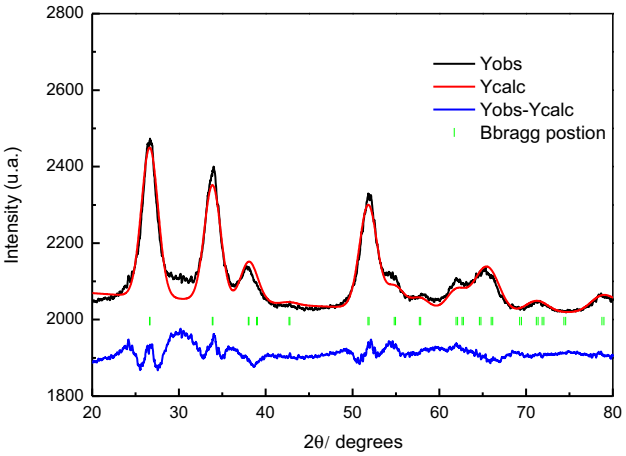

Fig. 1 – X-ray diffraction pattern of Sb-doped $Sn_{0.9}Sb_{0.1}O_2$ (ATO) synthesized and calcined at 500 °C for 12 h, and its corresponding Rietveld refinement plot. Space group P42/mnm, a = 4.7338 Å, b = 4.7338 Å, c = 3.1928, $\alpha = 90°$, $\beta = 90°$, $\gamma = 90°$, $\chi^2 = 0.8$, $R_{wp} = 0.22$, $R_p = 0.292$, $R_{exp} = 0.5076$.

Surface area and pore volume values estimated through the BJH method (c = 0.8) resulted in values of 115.17 m^2g^{-1} and 0.272 $cm^3\ g^{-1}$, respectively, for ATO; while the reported values for Ebonex® are 1.17 m^2g^{-1} and 0.01 cm^3g^{-1} [43]. The analysis of the pore size distribution (N_2 desorption branch) indicated the presence of mesopores in the ATO support. It is remarkable that the surface area value obtained for ATO support is superior to the value of the catalytic material [15]. The ATO support could provide a possible effective method for the dispersion of catalytic materials on the substrate as opposed to current method of commercially available Ebonex®. It is expected that ATO will have a contribution in the performance.

Fig. 2 shows the TEM micrographs; spherical aggregates and networks can be seen. A careful analysis of several micrographs allows the estimation of the mean diameters of the primary particles (Fig. 2B). The average particle size was 4.4 nm. The mean sizes were comparable with the results obtained by XRD.

Fig. 3 shows the EIS spectrum under PEMFC and PEMWE modes at 80 °C and atmospheric pressure. Under these conditions the oxygen reactions represent the determining step and the hydrogen electrode can be assumed to act as pseudo-reference electrode [44]. The value of the series resistance (R_s) was 0.27 $\Omega \cdot cm^2$ for Pt–IrO_2/ATO in PEMFC mode, whereas the charge transference resistance (R_{ct}) was 4.5 $\Omega \cdot cm^2$. In PEMWE mode, the R_s was 0.28 $\Omega \cdot cm^2$ and the R_{ct} was 2.38 $\Omega \cdot cm^2$. The R_s values were similar to those obtained from commercial Ebonex® according to Siracusano et al.; however, the R_{ct} value was lower than that reported in PEMWE mode [43].

Table 1 – XRF results of ATO support.

Sn %	Sb %	Cl %
90.1	9.1	0.8

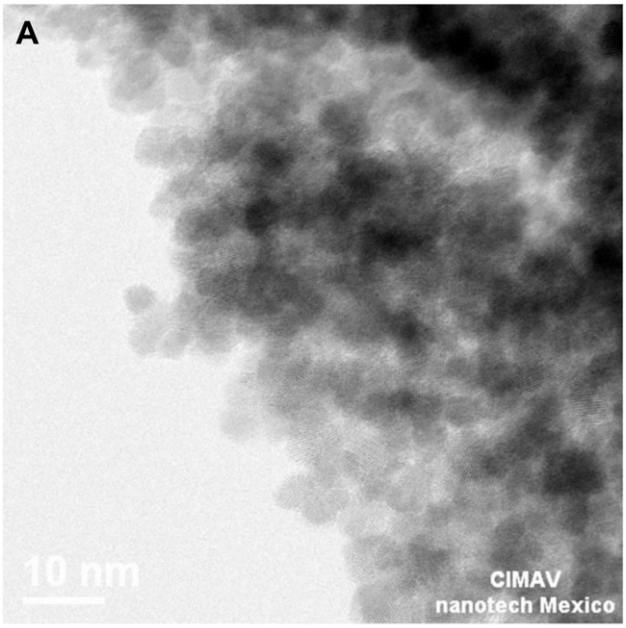

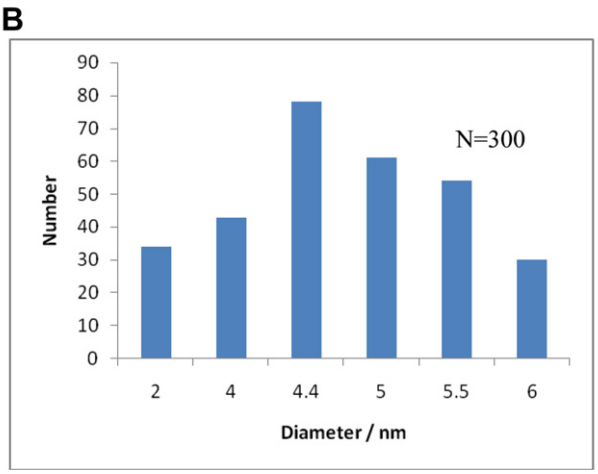

Fig. 2 – TEM micrographs of ATO support: (A) and (B) Particle size distribution analysis.

The performance of the MEA based on the Pt–IrO_2/ATO system for oxygen evolution/reduction reactions was evaluated at 80 °C for both PEMWE and PEMFC (Fig. 4). The PEMWE performance is higher than that obtained when commercial Ebonex® and Ti_nO_{2n-1} were used as the catalyst support [43]. At 1.8 V, these are 300 A g^{-1} and 700 A g^{-1} for IrO_2/Ebonex® and IrO_2/Ti_nO_{2n-1}, respectively; meanwhile at same cell voltage a mass activity value of 1118 A g^{-1}, corresponding to Pt–IrO_2 supported on ATO was achieved. The overpotential at the onset of the OER was 1.42 V versus 1.40 V for Ebonex® [33]. In the PEMFC mode, however, higher activity was observed for the ORR by the support materials than the ATO support; the mass activity was 565 A g^{-1} at 0.3 V and 80 °C. It is possible that the ATO support participates in the OER in PEMWE mode in acid media according to C. Xiao et al. [45], but not for the ORR in PEMFC mode. According to different authors, including Damjanovic, Brusic, and Know [46–50]; this result may be attributed to the contribution of surface oxide formation on Pt,

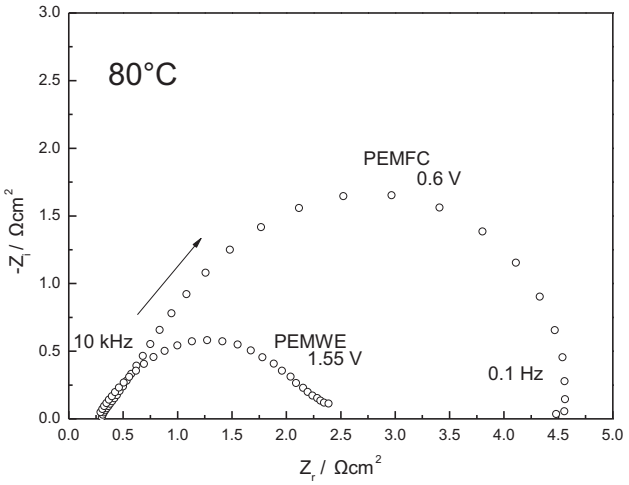

Fig. 3 – IES spectra of Pt–IrO_2/ATO support in PEMFC mode (0.6 V) and PEMWE mode (1.55 V) at 80 °C.

it has been shown that for a potential near 0.8 V versus NHE there is a type of oxygen adsorption on the surface of the Pt (Pt–O). Beside this, Thacker and Hoare [49] demonstrated that for potentials between 1 and 2 V versus NHE, certain Pt–O sites may react to become PtO_2 or, in the presence of O_2, and the interaction of the gas with the surface of the Pt may cause Pt–O_2 to form. This possible explanation can be attributed to the contribution of the Pt material, due to surface oxides created by the potential, which works in PEMWE, because it is known that PtOx is active for OER [51]. This finding is not observed in PEMFC, since IrO_2 and support (ATO) are not active in carrying out the ORR and may block active Pt sites, decreasing the performance of the system in this modality.

Fig. 5 shows chronoamperometric curves from testing, which was carried out at 80 °C and atmospheric pressure for the Pt–IrO_2/ATO materials. These experiments were performed by applying a potential of 0.6 V for 400 min in PEMFC mode, and subsequently at 1.55 V for the same amount of time in PEMWE mode. The results showed an acceptable stability for this lapse of time in the two different functions.

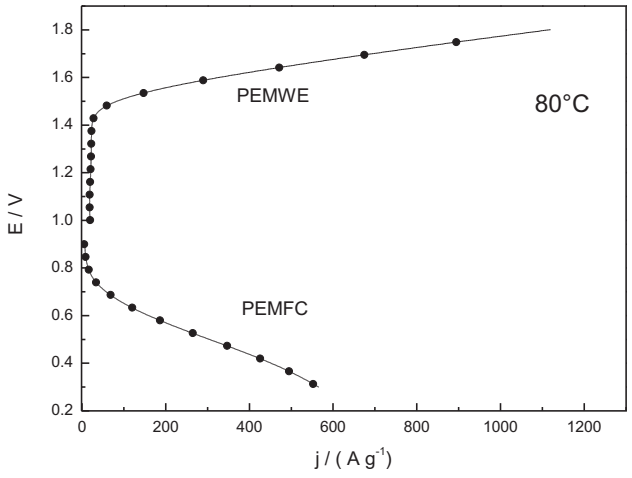

Fig. 4 – URFC polarization curves at 80 °C created with the MEA based on the Pt–IrO_2/ATO material.

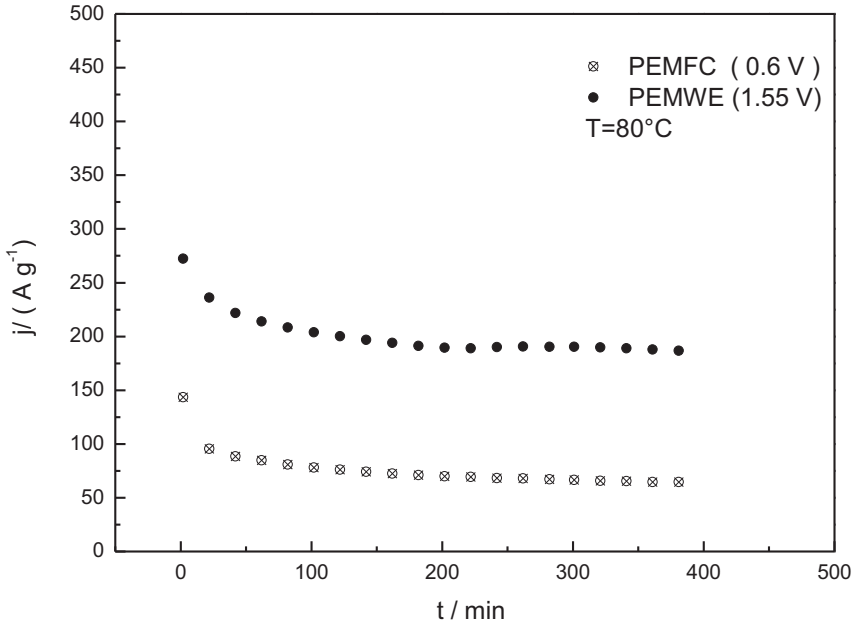

Fig. 5 – Chronoamperometric curves of Pt–IrO_2/ATO material in PEMFC and PEMWE modes at 0.6 V and 1.55 V, respectively, at 80 °C.

The round-trip energy conversion efficiencies (ε_{RT}) during water electrolysis and fuel-cell operation using the ATO support were calculated with the following equation at different current densities [52–54]:

$$\varepsilon_{RT} = \frac{E_{FC}}{E_{WE}}, \quad (1)$$

where E_{FC} and E_{WE} are the cell voltages of the fuel cell and water electrolyser, respectively, at a given current density. The values of round-trip energy efficiency were approximately 48%, 43% and 31% at 50, 100 and 200 A g^{-1}, respectively.

4. Conclusions

A support based on Sb-doped SnO_2 (ATO) for PEM-URFC has shown promising properties in the PEMWE mode in comparison with an Ebonex® commercial support. The crystal size obtained through this synthesis procedure was 4–6 nm. The surface values estimated by means of the BET method for ATO are significantly higher than the values obtained for commercial ATO and Ebonex®. Furthermore, the maximum mass current activity was 1118 A g^{-1} at 1.8 V in PEMWE mode (Water electrolyser) and 565 A g^{-1} at 0.3 V in PEMFC mode (Fuel cell), both at 80 °C. The value for round-trip energy efficiency was approximately 48% at 50 A g^{-1}.

Acknowledgments

The authors thank the Mexican Council for Science and Technology CONACYT for financial support through SEP-CONACYT 2009-133310. Thanks to Tozzi Renewable Energy SpA for financial support. We also thank to CIMAV for TEM measurements J. C. Cruz. Alvarez acknowledges to CONACYT for a graduate scholarship.

REFERENCES

[1] Grigoriev SA, Porembsky VI, Fateev VN. Pure hydrogen production by PEM electrolysis for hydrogen energy. Int J Hydrogen Energy 2006;31:171–5.
[2] Cheng J, Zhang H, Chen G, Zhang Y. Study of $IrxRu_1-xO_2$ oxides as anodic electrocatalysts for solid polymer electrolyte water electrolysis. Electrochim Acta 2009;54:6250–6.
[3] Marshall AT, Sunde S, Tsypkin M, Tunold R. Performance of a PEM water electrolysis cell using $Ir_xRu_yTa_zO_2$ electrocatalysts for the oxygen evolution electrode. Int J Hydrogen Energy 2007;32:2320–4.
[4] Barbir F. PEM electrolysis for production of hydrogen from renewable energy sources. Sol Energy 2005;78:661–9.
[5] Shidong S, Huamin Z, Xiaoping M, Zhigang S, Baker RT, Yi B. Electrochemical investigation of electrocatalysts for the oxygen evolution reaction in PEM water electrolyzers. Int J Hydrogen Energy 2008;33:4955–61.
[6] Tseng ChJ, Lo SK. Effects of microstructure characteristics of gas diffusion layer and microporous layer on the performance of PEMFC. Energ Convers Manage 2010;51:677–84.
[7] Yousfi-Steiner N, Moçotéguy Ph, Candusso D, Hissel D. A review on polymer electrolyte membrane fuel cell catalyst degradation and starvation issues: causes, consequences and diagnostic for mitigation. J Power Sources 2009;194:130–45.
[8] Oh HS, Oh JG, Kim H. Modification of polyol process for synthesis of highly platinum loaded platinum–carbon catalysts for fuel cells. J Power Sources 2008;183:600–3.

[9] Brady MP, Wang H, Yang B, Turner JA, Bordignon M, Molins R, et al. Growth of Cr-Nitrides on commercial Ni–Cr and Fe–Cr base alloys to protect PEMFC bipolar plates. Int J Hydrogen Energy 2007;32:3778–88.

[10] Ye ZG, Meng HM, Sun DB. Electrochemical impedance spectroscopic (EIS) investigation of the oxygen evolution reaction mechanism of $Ti/IrO_2 + MnO_2$ electrodes in 0.5 m H_2SO_4 solution. J Electroanal Chem 2008;621:49–54.

[11] Gaudet J, Tavares AC, Trasatti S, Guay D. Physicochemical characterization of mixed RuO_2-SnO_2 solid solutions. Chem Mater 2005;17:1570–9.

[12] Hutchings R, Müller K, Kotz R, Stucki S. A structural investigation of stabilized oxygen evolution catalysts. J Mater Sci 1984;19:3987–94.

[13] Ito M, Murakami Y, Hayato K, Hiroyuki O, Kiyochika Y, Yoshio T. Preparation of ultrafine RuO_2-SnO_2 binary oxide particles by a sol-gel process. J Electrochem Soc 1994;141(5): 1242–5.

[14] Jirkovský J, Makarova M, Krtil P. Particle size dependence of oxygen evolution reaction on nanocrystalline RuO_2 and $Ru_{0.8}Co_{0.2}O_{2-x}$. Electrochem Commun 2006;8:1417–22.

[15] Cruz JC, Baglio V, Siracusano S, Ornelas R, Ortiz-Frade L, Arriaga LG, et al. Nanosized IrO_2 electrocatalysts for oxygen evolution reaction in an SPE electrolyzer. J Nanopart Res 2011;13:1639–46.

[16] Marshall A, Børresen B, Hagen G, Sunde S, Tsypkin M, Tunold R. Iridium oxide-based nanocrystalline particles as oxygen evolution electrocatalysts. Russ J Electrochem 2006; 42:1134–40.

[17] Hu C-C, Wen T-C. Voltammetric investigation of palladium oxides III: effects of hydration and pH on the electrocatalytic properties of Pd(IV)Pd(II) and the reduction behaviour of palladous oxid. Electrochim Acta 1996;41:1505–14.

[18] Hu C-C, Liu K-Y. Voltammetric investigation of platinum oxides. I. Effects of ageing on their formation/reduction behavior as well as catalytic activities for methanol oxidation. Electrochim Acta 1999;44:2727–38.

[19] Rudorff W, Luginsland H-H, Anorg Z. Untersuchungen an ternären Oxiden der Übergangsmetalle. II. Die Systeme TiO_2-NbO_2 und TiO_2- $TiTaO_4$. Allg Chem 1964;334:125–41.

[20] Arbiol J, Cerda J, Dezanneau G, Cirera A, Peiro F, Cornet A, et al. Effects of Nb doping on the TiO anatase-to-rutile phase transition. J Appl Phys 2002;92:853–61.

[21] García BL, Fuentes R, Weidner JW. Low-temperature synthesis of a PtRu/ NbTiO electrocatalyst for methanol oxidation. Electrochem Solid State Lett 2007;10:B108–10.

[22] Ganesan R, Lee JS. An electrocatalyst for methanol oxidation based on tungsten trioxide microspheres and platinum. J Power Sources 2006;157:217–21.

[23] Cui X, Shi J, Chen H, Zhang L, Guo L, Gao J, et al. Platinum/ Mesoporous WO_3 as a carbon-Free electrocatalyst with enhanced electrochemical activity for methanol oxidation. J Phys Chem B 2008;112:12024–31.

[24] Rajeswari J, Viswanathan B, Varadarajan TK. Tungsten trioxide nanorods as supports for platinum in methanol oxidation. Mater Chem Phys 2007;106:168–74.

[25] Maiyalagan T, Viswanathan B. Catalytic activity of platinum/ tungsten oxide nanorod electrodes towards electro-oxidation of methanol. J Power Sources 2008;175:789–93.

[26] Suzuki Y, Ishihara A, Mitsushima S, Kamiya N, Ota K. Sulfated-zirconia as a support of Pt catalyst for polymer electrolyte fuel cells. Electrochem Solid State Lett 2007;10: B105–7.

[27] Chhina H, Campbell S, Kesler O. An oxidation-resistant indium tin oxide catalyst support for proton exchange membrane fuel cells. J Power Sources 2006;161:893–900.

[28] Zhang S, Zhu H, Yu H, Hou J, Yi B, Ming P. The oxidation resistance of tungsten carbide as catalyst support for proton exchange membrane fuel cells. Chin J Catal 2007;28:109–11.

[29] Chhina H, Campbell S, Kesler O. Thermal and electrochemical stability of tungsten carbide catalyst supports. J Power Sources 2007;164:431–40.

[30] Scott K, Cheng H. The anodic behaviour of Ebonex_ in oxalic acid solutions. J Appl Electrochem 2002;32:583–9.

[31] Vračar LjM, Krstajić NV, Radmilović VR, Jakšić MM. Electrocatalysis by nanoparticles – oxygen reduction on Ebonex/Pt electrode. J Electroanal Chem 2006;587:99–107.

[32] Paunović P, Popovski O, Fidančevska E, Ranguelov B, Gogovsk DS, Dimitrov AT, et al. Co-Magneli phases electrocatalysts for hydrogen/oxygen evolution. Int J Hydrogen Energy 2010;35:10073–80.

[33] Escalante-García IL, Duron-Torres SM, Cruz JC, Arriaga-Hurtado LG. Electrochemical characterization of IrO_2-Pt and RuO_2-Pt mixtures as bifunctional electrodes for unitized regenerative fuel cells. J New Mat Electr Sys 2010; 13:227–33.

[34] Tuseeva EK, Mayorova NA, Sosenkin VE, Nikol'skaya NF, Vol'fkovich YM, Krestinin AV, et al. Carbon nanotubes as a support for Pt- and Pt–Ru-catalysts of reactions proceeding in fuel cells. Russ J Electrochem 2008;44:884–93.

[35] Antolini E, Gonzalez ER. Ceramic materials as support for low-temperature fuel cell catalysts. Solid State Ionics 2009; 180:746–63.

[36] Vicent F, Morallón E, Quijada C, Vázquez JL, Aldaz A. Characterization and stability of doped SnO_2 anodes. J Appl Electrochem 1998;28:607–12.

[37] Marshall AT, Haverkamp RG. Electrocatalytic activity of IrO_2–RuO_2 supported on Sb doped SnO_2 nanoparticles. Electrochim Acta 2010;55:1978–84.

[38] Wu X, Scott K. RuO_2 supported on Sb-doped SnO_2 nanoparticles for polymer electrolyte membrane water electrolysers. Int J Hydrogen Energy 2010;30:1–5.

[39] Rietveld HM. Profile refinement method for nuclear and magnetic structures. J Appl Crystallogr 1969;2:65–71.

[40] Rodriguez-Carvajal Y. Recent advances in magnetic structure determination by neutron powder diffraction. Physica B 1993;192:55–69.

[41] Mazumder V, Lee Y, Sun S. Recent development of active nanoparticle catalysts for fuel cell reactions. Adv Func Mater 2010;20:1224–31.

[42] Zhi Qun T, San Ping J, Zengcai L, Lin L. Polyelectrolyte-stabilized Pt nanoparticles as new electrocatalysts for low temperature fuel cells. Electrochem Commun 2007;9:1613–8.

[43] Siracusano S, Baglio V, D'Urso C, Antonucci V, Aricò AS. Preparation and characterization of titanium suboxides as conductive supports of IrO_2 electrocatalysts for application in SPE electrolysers. Electrochim Acta 2009;54:6292–9.

[44] Cooper KR, Ramani V, Fenton JM, Kunz HR. Experimental methods and data analyses for polymer electrolyte fuel cells. Southern Pines, North Carolina: Scribner Associates Inc.; 2004–2005.

[45] Xiao C, Guohua Z, Yanzhu L, Hongxu L, Peigiang L, Meichuan L. Novel vertically aligned TiO_2 nanotubes embedded with Sb-dopped SnO_2 electrode with high oxygen evolution potential and long service time. Mat Chem Phys 2009;113:314–21.

[46] Schuldiner S, Warner TB, Piersma BJ. Potentiostatic current-potential measurements on a platinum electrode in a high-purity closed system. J Electrochem Soc 1967;114:343–9.

[47] Damjanovic A, Dey A, Bockris JOM. Kinetics of oxygen evolution and dissolution on platinum electrodes. Electrochim Acta 1966;11:791–814.

[48] Schuldiner S, Roe RM. Transition from hydrogen ionization to oxygen evolution on a platinum electrode. J Electrochem Soc 1963;110:332–8.

[49] Thacker R, Hoare JP. Sorption of oxygen from solution by noble metals: I. Bright platinum. J Electroanal Chem Interf Chem 1971;30:1–14.

[50] Wroblowa H, Rao MLB, Damjanovic A, Bockris JOM. Adsorption and kinetics at platinum electrodes in the presence of oxygen at zero net current. J Electroanal Chem Interf Chem 1967;15:139–50.
[51] Man IC, Su H-Y, Calle-Vallejo F, Hansen HA, Martínez JI, Inoglu NG, et al. Universality in oxygen evolution electrocatalysis on oxide surfaces. ChemCatChem 2011;7: 1159–65.
[52] Pettersson J, Ramsey B, Harrison D. A review of the latest developments in electrodes for unitised regenerative polymer electrolyte fuel cells. J Power Sources 2006;157:28–34.
[53] Kiyosi K, Yoshito F. Sputter deposited Pt-Ir oxides thin films and their characterization. Mater Sci Eng B 2004;109:188–91.
[54] Singh RN, Mishra D, Anindita A, Sinha SK, Singh A. Novel electrocatalysts for generating oxygen from alkaline water electrolysis. Electrochem Commun 2007;9:1369–73.